14th International Symposium on Turbulence and Shear Flow Phenomena (TSFP14)
Heidelberg, Germany, July 28–31, 2026

PHYSICS-GUIDED ADAPTIVE CORRECTION FOR DATA-DRIVEN TURBULENCE MODELING

Seoyeon Heo, Yeji Yun, Junho Eom, Solkeun Jee
School of Mechanical and Robotics Engineering
Gwangju Institute of Science and Technology
Gwangju, South Korea
hsy50952@gm.gist.ac.kr

ABSTRACT

Typical Reynolds-averaged Navier–Stokes (RANS) models remain unreliable in predicting separated flow, secondary flow, and adverse-pressure-gradient flow, although they are well validated for attached boundary layers with mild pressure gradients. It is critical to identify such questionable flow regions for turbulence model improvement. This study proposes a physics-based classifier to mark uncertain flow regions for a general RANS model. Then, a baseline RANS model is corrected through the field inversion process only in the uncertain region. Such model correction is conducted adaptively to the identified uncertain region. The proposed framework of adaptive field inversion retains the accuracy of the baseline turbulence model in attached boundary layers and captures challenging flow phenomena such as flow separation.

INTRODUCTION

Conventional Reynolds-averaged Navier–Stokes (RANS) models are uncertain in predicting complex flows, including separated, secondary, and adverse-pressure-gradient flows, as they are primarily designed for well-attached boundary layer. Recently, data-driven approaches have been widely employed to improve RANS predictions for such uncertain flows. The field inversion and machine learning (FIML) framework [Parish & Duraisamy (2016)] is one of the widely adopted frameworks for data-driven RANS modeling. The FIML framework consists of two stages: field inversion and machine learning. The field inversion stage provides optimal corrections to RANS equations. The machine learning stage then generalizes the RANS corrections.

However, data-driven RANS modeling frameworks occasionally degrade accuracy in well-validated attached flows, such as zero-pressure gradient boundary layers. This limitation also appears in the FIML method. The nominal field inversion takes the whole computational domain for optimizing a RANS model. Here, the nominal method is called full-field inversion. The full-field inversion often modifies well-attached flow to satisfy a given optimization goal. Our previous study [Heo *et al.* (2024, 2025)] employed a zonal method in which the field inversion region was manually specified to shield the attached boundary layer. However, this manual approach is impractical for complex geometries, where the reliability of RANS predictions cannot be known in advance.

This study proposes an adaptive correction method for data-driven RANS modeling, comprising two key processes: (1) identification of uncertain regions in a baseline RANS model using a physics-based classifier and (2) adaptive correction of the baseline model in the identified uncertain regions.

METHODOLOGY

Physics-Based Classifier

A physics-based classifier is designed to identify an uncertain region where a RANS model may require a model correction process (here, field inversion is used for the model correction). The classifier leverages well-established boundary-layer physics using 5 local flow parameters defined in Eq. 1.

$$\begin{aligned}
\phi_1 &= \kappa d, \\
\phi_2 &= \frac{\kappa\Omega}{\sqrt{\frac{\partial\Omega}{\partial x_i}\frac{\partial\Omega}{\partial x_i}}}, \\
\phi_3 &= \sqrt{\frac{\nu_t}{\Omega}}, \\
\phi_4 &= \left\|(S_{ik}W_{kj} - W_{ik}S_{kj})(1-\delta_{ij})\right\|, \\
\phi_5 &= \Omega
\end{aligned} \tag{1}$$

where d is the wall distance, Ω is the vorticity magnitude, ν_t is the kinematic eddy viscosity, S_{ij} is the strain-rate tensor, and W_{ij} is the rotation-rate tensor. Turbulent length scales are represented by flow parameters ϕ_1 through ϕ_3. The flow parameter ϕ_1 is the wall-distance-based length scale, ϕ_2 is the von Kármán length scale, and ϕ_3 is the eddy-viscosity-based length scale. Misalignment between the strain-rate and rotation-rate tensors is quantified by ϕ_4, and the vorticity magnitude is represented by ϕ_5.

The classification criteria are defined using ϕ_1–ϕ_5, as given in Eq. 2.

$$\begin{aligned}
C_1 &: \left|\frac{\phi_1}{\phi_3} - 1\right| < \tau_1, \\
C_2 &: \left|\frac{\phi_1}{\phi_2} - 1\right| < \tau_1, \\
C_3 &: \frac{\phi_4}{\phi_5} < \tau_2
\end{aligned} \tag{2}$$

The criteria C_1 and C_2 enforce consistency among the length scales ϕ_1–ϕ_3. These scales exhibit comparable magnitudes in attached turbulent boundary layers [Spalart & Allmaras (1992); Spalart *et al.* (2006); Xu *et al.* (2019)], ensuring that their ratios remain near unity within a threshold τ_1. Criterion C_3 evaluates the misalignment between the strain-rate and rotation-rate tensors through ϕ_4. These tensors are typically well-aligned in attached turbulent boundary layers [Spalart (2000)], resulting in ϕ_4 values significantly smaller than the vorticity magnitude ϕ_5 within a threshold τ_2. A region is classified as reliable only when all three criteria are satisfied simultaneously. Otherwise, it is classified as uncertain, as defined in Eq. 3. Please note that the proposed classifier is universally applicable to linear eddy-viscosity models, as it does not rely on model-specific parameters.

$$\mathscr{R}(x_i) = \begin{cases} \text{Reliable} & \text{if } C_1 \wedge C_2 \wedge C_3 \\ \text{Uncertain} & \text{otherwise} \end{cases} \tag{3}$$

Adaptive Field Inversion

The proposed physics-based classifier is coupled with the field inversion framework to enable adaptive model correction (i.e., adaptive field inversion). Model correction is restricted to uncertain regions, while a baseline model remains preserved within reliable regions. The Spalart–Allmaras (SA) model is used as the baseline model, as formulated in Eq. 4. The correction β modifies the net source term of the SA model.

$$\begin{aligned} \frac{D\hat{\nu}}{Dt} =& \beta\left(c_{b1}\hat{S}\hat{\nu} - c_{w1}f_w\left(\frac{\hat{\nu}}{d}\right)^2\right) \\ &+ \frac{1}{\sigma}\left[(\nu+\hat{\nu})\nabla^2\hat{\nu} + (1+c_{b2})\nabla\hat{\nu}\cdot\nabla\hat{\nu}\right] \end{aligned} \tag{4}$$

The condition $\beta = 1$ corresponds to the original SA model without correction. The optimal correction field β is obtained by minimizing the objective function defined in Eq. 5.

$$J(\beta) = \sum_{j=1}^{N_\zeta}\left(\zeta_{target,j} - \zeta_{RANS,j}\right)^2 + \lambda\sum_{i=1}^{N_p}(\beta_i - 1)^2 \tag{5}$$

where ζ is the flow quantity of interest, N_ζ is the number of the grid points associated with ζ, λ is the regularization factor, and N_p is the number of grid points in the field inversion domain — here only uncertain regions.

RESULTS AND DISCUSSION

Physics-Based Classifier

The performance of the proposed physics-based classifier is evaluated across four representative flow configurations to assess its robustness and general applicability. The test cases include (1) sharp-corner separation around an axisymmetric body, (2) shock-induced separation over a transonic bump, (3) free shear flow in a cold axial jet, and (4) secondary flow in a three-dimensional duct. Each configuration involves distinct flow physics and is known to challenge conventional RANS models. In all cases, the classification is restricted to regions with sufficiently turbulent flow, based on $\mu_t/\mu > 10$.

The sharp-corner separation around an axisymmetric body [Herrin & Dutton (1994)] is the first test case, as shown in Fig. 1. The incoming turbulent boundary layer remains attached to the upstream wall before undergoing abrupt separation at the sharp base corner. A recirculation bubble subsequently forms downstream of the corner. Typical RANS models often fail to accurately predict the base pressure and the size of the recirculation bubble in this configuration [Herrin & Dutton (1994); Kawai & Fujii (2005); Heo *et al.* (2025)]. The classifier identifies the upstream attached boundary layer as a reliable region. Similarity among the three length scales and the alignment of the strain-rate and rotation-rate tensors characterize this reliable state. The separated flow downstream of the corner is identified as an uncertain region where the predictive reliability of the RANS decreases.

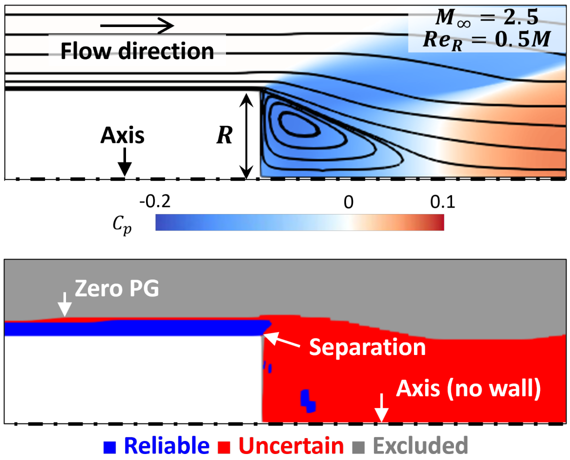

Figure 1: Flow configuration and region identification for sharp-corner separation around an axisymmetric body.

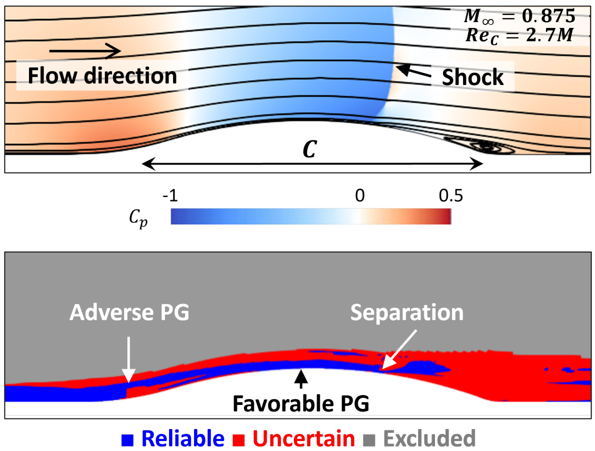

Figure 2: Flow configuration and region identification for shock-induced separation over a transonic bump.

Shock-induced separation over an axisymmetric bump [Bachalo & Johnson (1986)] is examined, as shown in Fig. 2. The incoming turbulent boundary layer encounters concave curvature at the onset of the bump, inducing a localized adverse pressure gradient. The flow then accelerates over the subsequent convex surface under a favorable pressure gradient. As the flow accelerates, a shock wave forms on the bump, leading to flow separation and the formation of a recirculation bubble. Conventional RANS models often show discrepancies in predicting the shock location and the size of the recirculation bubble [Spalart *et al.* (2017); Uzun & Malik (2019)]. The physics-based classifier identifies the upstream attached boundary layer and the favorable pressure gradient region as reliable. Uncertain regions encompass the adverse pressure gradient region at the bump onset and the separated region after the shock.

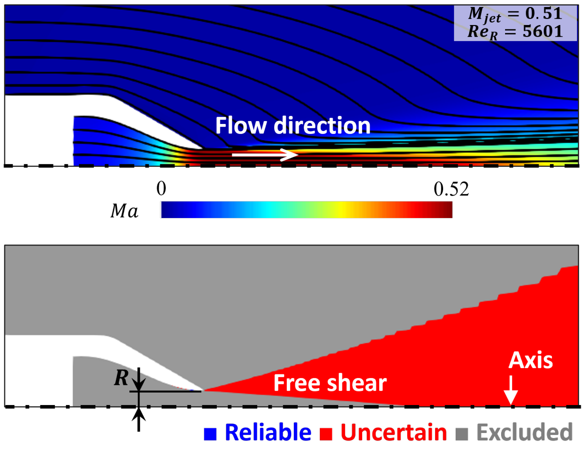

Figure 3: Flow configuration and region identification for free shear flow in an axial jet.

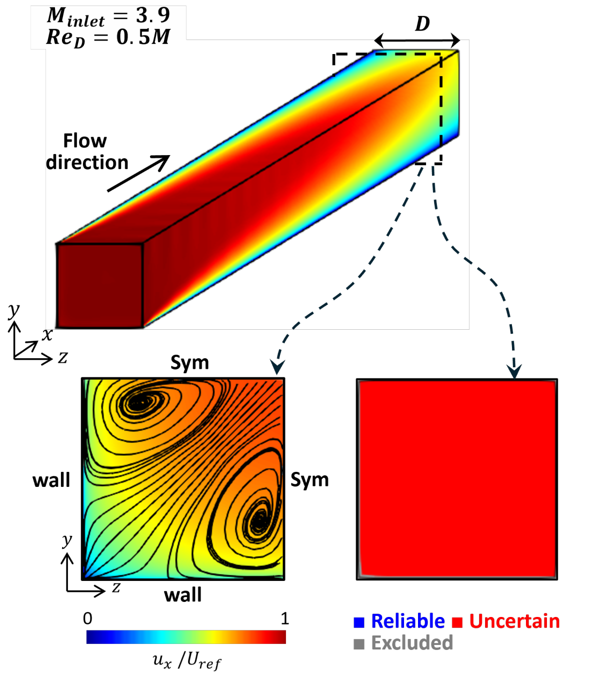

Figure 4: Flow configuration and region identification for secondary flow in a three-dimensional duct.

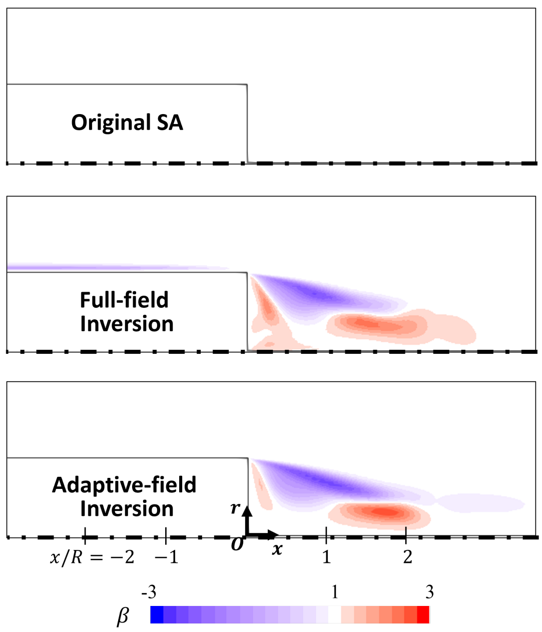

Figure 5: SA correction β fields from the original SA, full-field inversion, and adaptive-field inversion.

Free shear flow in an axial jet [Bridges & Wernet (2011)] serves as the third test case to assess the classifier in a non-wall-bounded environment (Fig. 3). A subsonic jet discharging into ambient fluid characterizes this configuration. A free shear layer forms at the interface between the jet and the ambient flow, resulting in strong velocity gradients. The jet gradually spreads as the surrounding fluid is entrained into the shear layer downstream. Standard RANS models often exhibit significant inaccuracies in predicting the jet spreading rate [Yoder *et al.* (2015); Dudek (2019)]. The classifier identifies most of the flow domain as an uncertain region because the flow is dominated by free shear flow throughout.

Secondary flow within a three-dimensional square duct [Davis & Gessner (1989)] is examined (see Fig. 4). Secondary vortices develop due to the non-circular duct geometry. Conventional *linear* RANS models are inherently unable to predict the strength and velocity of these secondary vortices. The physics-based classifier identifies most of the flow domain as an uncertain region. Misalignment between the strain-rate and rotation-rate tensors ϕ_4 triggers this classification.

Adaptive-field inversion

The adaptive field inversion is applied to the sharp-corner separation around an axisymmetric body. Conventional RANS models often fail to predict the base pressure. Experimental C_p data [Herrin & Dutton (1994)] at the base surface are used to define the target quantity $\zeta_{\text{target},j}$ in the objective function $J(\beta)$ (see Eq. 5). The adaptive field inversion defines the uncertain regions shown in Fig. 1 as the optimization domain, where the SA model is modified exclusively. In contrast, the full-field inversion applies the model correction over the entire domain.

Figure 5 compares the SA correction β fields for the original SA, full-field inversion, and adaptive-field inversion. The condition $\beta = 1$ corresponds to the original SA model without modification. In the full-field inversion, the model correction extends into the upstream attached boundary layer ($x < 0$). In contrast, the adaptive-field inversion confines the correction to the wake region downstream of the corner, leaving the upstream attached boundary layer unaltered.

Figure 6 shows the effect of the SA model correction on the eddy viscosity field for the original SA, full-field inversion, and adaptive-field inversion. Both full-field and adaptive-field inversion approaches reduce the eddy viscosity in the wake region compared to the original SA model. The upstream attached boundary layer reveals the primary distinction between the two field inversion methods. The adaptive-field inversion maintains eddy-viscosity levels comparable to the original SA model. The full-field inversion, however, significantly reduces the eddy viscosity in the upstream region, which is not desirable. Unwanted model modification within the upstream attached boundary layer represents a limitation of the full-field inversion.

Figure 7 compares the upstream velocity profiles. The adaptive-field inversion preserves the log-law behavior of the attached boundary layer, maintaining the accuracy of the orig-

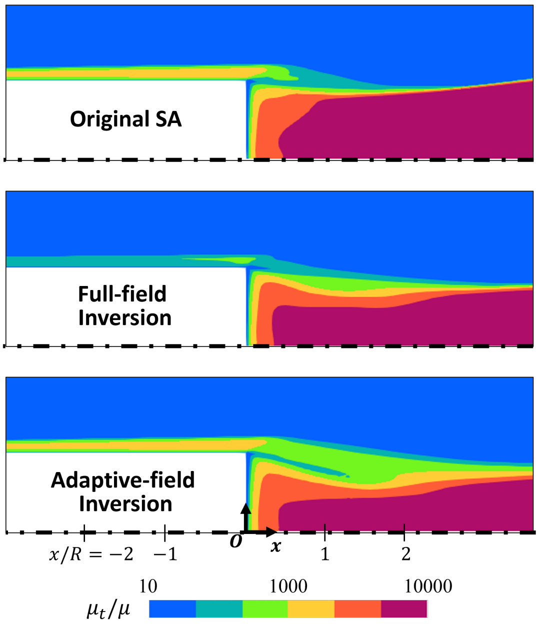

Figure 6: Eddy viscosity fields from the original SA, full-field inversion, and adaptive-field inversion.

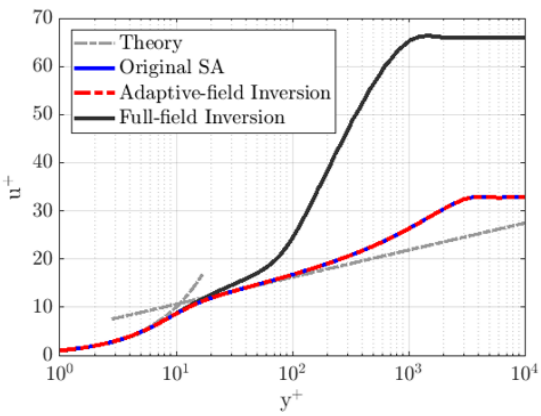

Figure 7: Upstream velocity profiles at $x/R = -0.02$ for sharp-corner separation from the original SA, full-field inversion, and adaptive-field inversion.

inal SA model. The full-field inversion shows a significant deviation from the expected turbulent boundary layer profile. This deviation is associated with an unphysical reduction in eddy viscosity in the upstream region, where the original SA prediction is already reliable.

Figure 8 compares the radial distribution of the base pressure coefficient. The adaptive-field inversion achieves close agreement with the experimental data, indicating that the optimization successfully improves the base pressure prediction. This improvement is obtained while preserving the upstream velocity profile. In contrast, although the full-field inversion also reduces the discrepancy with the experimental data, it does so at the expense of degrading the upstream boundary layer. These results demonstrate that the adaptive-field inversion effectively introduces model corrections in the wake region while maintaining the accuracy of the upstream flow.

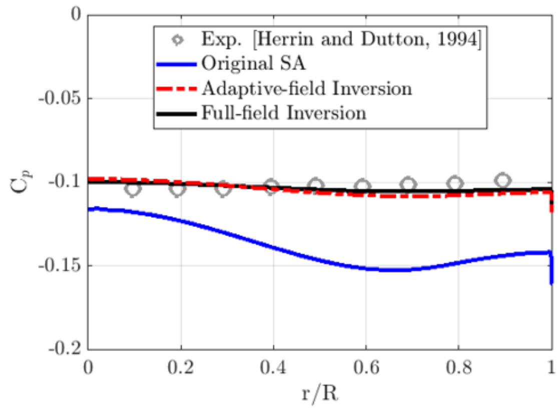

Figure 8: Radial distribution of the base pressure C_p for sharp-corner separation from the original SA, full-field inversion, and adaptive-field inversion.

CONCLUSIONS

The physics-guided adaptive correction method is proposed in this study for a RANS turbulence model. The physics-based classifier is designed to determine whether a certain flow region in a RANS solution is reliable or uncertain. The classifier employs local flow parameters that represent boundary-layer physics. Since the flow parameters do not include model-specific quantities, the classifier is universally applicable to linear eddy-viscosity models. The classifier is coupled with the field inversion framework to enable adaptive correction. Field inversion is used in this study to demonstrate adaptive model correction, while the classifier remains applicable to other data-driven modeling approaches. The current adaptive field inversion improves the prediction capability of a baseline RANS model for uncertain flow regions while maintaining the well-designed model performance for the attached boundary layer.

Acknowledgments

This work was supported by Data-Driven Flow Modeling Research Laboratory funded by Defense Acquisition Program Administration under Grant UD230015SD. This work was also supported by the National Research Foundation of Korea (NRF) grant funded by the Korea government (MSIT) (Project No. RS-2024-00438833), the Basic Science Research Program through the National Research Foundation of Korea (NRF) funded by the Ministry of Education (Project No. RS-2025-25433522), and the GIST-IREF program from Gwangju Institute of Science and Technology (GIST).

REFERENCES

Bachalo, WDF & Johnson, DA 1986 Transonic, turbulent boundary-layer separation generated on an axisymmetric flow model. *AIAA journal* **24** (3), 437–443.

Bridges, James & Wernet, Mark P 2011 The NASA subsonic jet particle image velocimetry (PIV) dataset. *Tech. Rep.*.

Davis, DO & Gessner, FB 1989 Further experiments on supersonic turbulent flow development in a square duct. *AIAA journal* **27** (8), 1023–1030.

Dudek, Julianne 2019 Evaluation of full reynolds stress turbulence models in fun3d for axisymmetric jet flow. In *AIAA Scitech 2019 Forum*, p. 2332.

Heo, S., Kim, Y., Yun, Y. & Jee, S. 2025 Data-augmented turbulence modeling for separated compressible flow around axisymmetric bodies. *Aerospace Science and Technology* **166**, 110569.

Heo, S., Yun, Y., Jeong, M. & Jee, S. 2024 Simulation of supersonic axisymmetric base flow with a data-driven turbulence model. *Aerospace Science and Technology* **147**, 109014.

Herrin, J.L. & Dutton, J.C. 1994 Supersonic base flow experiments in the near wake of a cylindrical afterbody. *AIAA Journal* **32** (1), 77–83.

Kawai, Soshi & Fujii, Kozo 2005 Computational study of a supersonic base flow using hybrid turbulence methodology. *AIAA Journal* **43** (6), 1265–1275.

Parish, E.J. & Duraisamy, K. 2016 A paradigm for data-driven predictive modeling using field inversion and machine learning. *Journal of Computational Physics* **305**, 758–774.

Spalart, Philippe & Allmaras, Steven 1992 A one-equation turbulence model for aerodynamic flows. In *AIAA 30th Aerospace Sciences Meeting and Exhibit*, p. 439. AIAA 1992-439.

Spalart, Philippe R 2000 Strategies for turbulence modelling and simulations. *International Journal of Heat and Fluid Flow* **21** (3), 252–263.

Spalart, Philippe R, Belyaev, Kirill V, Garbaruk, Andrey V, Shur, Mikhail L, Strelets, Mikhail Kh & Travin, Andrey K 2017 Large-eddy and direct numerical simulations of the Bachalo-Johnson flow with shock-induced separation. *Flow, Turbulence and Combustion* **99** (3), 865–885.

Spalart, Philippe R, Deck, Shur, Shur, Michael L, Squires, Kyle D, Strelets, M Kh & Travin, Andrei 2006 A new version of detached-eddy simulation, resistant to ambiguous grid densities. *Theoretical and Computational Fluid Dynamics* **20** (3), 181–195.

Uzun, Ali & Malik, Mujeeb R 2019 Wall-resolved large-eddy simulations of transonic shock-induced flow separation. *AIAA Journal* **57** (5), 1955–1972.

Xu, Chang-Yue, Zhang, Tong, Yu, Yuan-Yuan & Sun, Jian-Hong 2019 Effect of von Kármán length scale in scale adaptive simulation approach on the prediction of supersonic turbulent flow. *Aerospace Science and Technology* **86**, 630–639.

Yoder, Dennis A, DeBonis, James R & Georgiadis, Nicholas J 2015 Modeling of turbulent free shear flows. *Computers & fluids* **117**, 212–232.